Earth and Planetary Science Letters 472 (2017) 1–13

Contents lists available at ScienceDirect

Earth and Planetary Science Letters

www.elsevier.com/locate/epsl

Ocean forcing of Ice Sheet retreat in central west Greenland from LGM to the early Holocene

Anne E. Jennings [a,*], John T. Andrews [a,b], Colm Ó Cofaigh [c], Guillaume St. Onge [d], Christina Sheldon [e], Simon T. Belt [f], Patricia Cabedo-Sanz [f], Claude Hillaire-Marcel [g]

[a] INSTAAR, University of Colorado, Boulder, CO 80309, USA
[b] Department of Geological Sciences, University of Colorado, Boulder, CO 80309, USA
[c] Department of Geography, Durham University, Science Site, South Road, Durham, DH1 3LE, UK
[d] Institut des sciences de la mer de Rimouski (ISMER) & GEOTOP, Université du Québec à Rimouski, 310, allée des Ursulines, Rimouski, Québec, G5L 3A1, Canada
[e] Centre for Past Climate Studies and Arctic Research Centre, Department of Geoscience, Aarhus University, Aarhus, Denmark
[f] Biogeochemistry Research Centre, School of Geography, Earth and Environmental Sciences, Plymouth University, Drake Circus, Plymouth, PL4 8AA, UK
[g] GEOTOP-UQAM, Montreal, QC, Canada

ARTICLE INFO

Article history:
Received 19 September 2016
Received in revised form 4 May 2017
Accepted 7 May 2017
Available online xxxx
Editor: M. Frank

Keywords:
central west Greenland
Greenland Ice Sheet
Baffin Bay
LGM
foraminifera
ocean forcing

ABSTRACT

Three radiocarbon dated sediment cores from trough mouth fans on the central west Greenland continental slope were studied to determine the timing and processes of Greenland Ice Sheet (GIS) retreat from the shelf edge during the last deglaciation and to test the role of ocean forcing (i.e. warm ocean water) thereon. Analyses of lithofacies, quantitative x-ray diffraction mineralogy, benthic foraminiferal assemblages, the sea-ice biomarker IP_{25}, and $\delta^{18}O$ of the planktonic foraminifera *Neogloboquadrina pachyderma* sinistral from sediments in the interval from 17.5–10.8 cal ka BP provide consistent evidence for ocean and ice sheet interactions during central west Greenland (CWG) deglaciation. The Disko and Uummannaq ice streams both retreated from the shelf edge after the last glacial maximum (LGM) under the influence of subsurface, warm Atlantic Water. The warm subsurface water was limited to depths below the ice stream grounding lines during the LGM, when the GIS terminated as a floating ice shelf in a sea-ice covered Baffin Bay. The deeper Uummannaq ice stream retreated first (ca. 17.1 cal ka BP), while the shallower Disko ice stream retreated at ca. 16.2 cal ka BP. The grounding lines were protected from accelerating mass loss (calving) by a buttressing ice shelf and by landward shallowing bathymetry on the outer shelf. Calving retreat was delayed until ca. 15.3 cal ka BP in the Uummannaq Trough and until 15.1 cal ka BP in the Disko Trough, during another interval of ocean warming. Instabilities in the Laurentide, Innuitian and Greenland ice sheets with outlets draining into northern Baffin Bay periodically released cold, fresh water that enhanced sea ice formation and slowed GIS melt. During the Younger Dryas, the CWG records document strong cooling, lack of GIS meltwater, and an increase in iceberg rafted material from northern Baffin Bay. The ice sheet remained in the cross-shelf troughs until the early Holocene, when it retreated rapidly by calving and strong melting under the influence of atmosphere and ocean warming and a steep reverse slope toward the deep fjords. We conclude that ocean warming played an important role in the palaeo-retreat dynamics of the GIS during the last deglaciation.

1. Introduction

Understanding the response of the Greenland Ice Sheet (GIS) to past large changes in climate and ocean forcing provides scope to place the dramatic current changes (e.g., Bamber et al., 2012; Enderlin et al., 2014) into a longer time-perspective and provides context for model predictions of future changes in the area and volume of the GIS. Currently, the GIS is losing mass by surface melt, runoff and ice discharge from outlet glaciers, with the total mass loss contributing to global sea level rise (Enderlin et al., 2014), and likely impacting on the Atlantic Meridional Overturning Circulation (Bamber et al., 2012). The GIS is complex, however, with many marine-terminating glaciers, which have a range of flow rates that vary with time (Rignot and Mouginot, 2012; Moon et al., 2012). Ocean forcing of grounding-line retreat has been documented in some of the fastest flowing of Greenland's outlet glaciers (e.g., Holland et al., 2008; Straneo et al., 2012), but the processes are complex and responses by individual outlet

* Corresponding author.
E-mail address: Anne.jennings@colorado.edu (A.E. Jennings).

http://dx.doi.org/10.1016/j.epsl.2017.05.007
0012-821X/

glaciers vary (cf. Joughin et al., 2012; Nick et al., 2009; Straneo and Heimbach, 2013; Rignot et al., 2015). Although these modern observations are compelling, the short time-period over which they span severely limits our ability to forecast GIS response to modern warming.

During the Last Glacial Maximum (LGM), the GIS advanced onto the continental shelf but it had retreated behind its present margin by the middle Holocene (cf. Funder et al., 2011; Larsen et al., 2015). Model reconstructions indicate an excess of ice equivalent sea level that reached a maximum of 5.1 m at 16.5 cal ka BP (Lecavalier et al., 2014), highlighting the large negative change in mass balance during deglaciation. Here, we present multi-proxy sediment core data on three previously unpublished sediment cores to reconstruct the LGM to Holocene GIS history of CWG, where some of the fastest flowing calving glaciers of the modern ice sheet enter the sea (Rignot et al., 2012). The cores are from the upper continental slope, beyond the maximum LGM extent of grounded ice at the shelf edge (Ó Cofaigh et al., 2013a, 2013b), thus allowing them to capture a sediment record of the oceanographic and environmental conditions that preceded and accompanied ice retreat. Importantly, such a perspective was lacking in earlier research where the timing of ice retreat was estimated based on (i) radiocarbon dates from outer shelf cores that record the timing of retreat already underway (Jennings et al., 2014; Sheldon et al., 2016) and (ii) radiocarbon dates from shells entrained in sediment gravity flows on the Disko trough mouth fan (TMF), which likely reflect remobilization of sediments by a Younger Dryas re-advance of Jakobshavns Isbrae (Ó Cofaigh et al., 2013b) rather than LGM ice activity. Building on this previous work, we address the following specific questions: When did the ice margin retreat from the shelf edge and did it retreat episodically, gradually or rapidly? Did ocean warming (Atlantic Water inflow) initiate and sustain retreat? Finally, we consider how the major events of GIS mass change recorded off CWG relate to the N. Hemisphere climate history recorded in the Greenland ice cores. Combined, we develop a conceptual model of GIS ice retreat and the drivers of retreat from the results of these analyses.

2. Environmental setting

Large cross-shelf troughs formed by fast flowing ice streams of the GIS terminate on the slope as major TMFs (Fig. 1) that accumulated during glacial–interglacial cycles (Hofmann et al., 2016a). The Uummannaq TMF is dominated in its upper part by glacigenic debris flows, deposited when the Uummannaq ice stream was last at the shelf edge during the LGM (Ó Cofaigh et al., 2013a; Dowdeswell et al., 2014). This cross-shelf trough joins the slope at c. 600 m water depth in a wide reentrant on the outer shelf (Fig. 1). By contrast, the Disko cross-shelf trough joins the slope at 350–400 m depth on the south side of the Disko TMF.

The West Greenland Current (WGC) is the source for warm ocean water along the western margin of the GIS, beginning where the East Greenland Current (EGC) and the Irminger Current (IC) become confluent as they round the southern tip of Greenland (Fig. 1). Cold, low salinity Polar Water originating in the EGC forms the surface layer close to the coast and is augmented by glacier melt as it proceeds northward (Ribergaard et al., 2008). Warmer, saline Atlantic Water originating in the IC flows below and west of the Polar Water (Buch, 2000a, 2000b) and, in Baffin Bay, forms the West Greenland Intermediate Water (WGIW) that submerges beneath the Arctic Surface Water (ASW) (Fig. 1) (Tang et al., 2004). These two components mix as they track northward along the shelf and shelf break and can enter the inner shelf and fjords, affecting outlets of the GIS grounded below sea level (Holland et al., 2008). The WGC is marked by lower sea-ice concentration and thickness along west Greenland (Tang et al., 2004). 'Vest-isen',

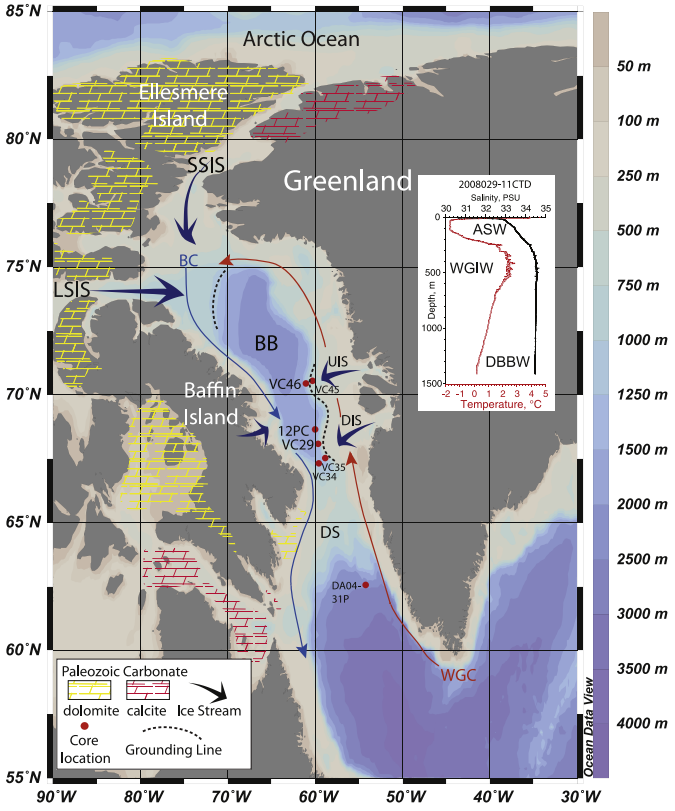

Fig. 1. Bathymetric map centered on Baffin Bay (BB) showing the locations of cores studied and mentioned in the text. Radiocarbon dates from cores JR175-VC45, -VC35, and -VC34 were used in previous studies to constrain the timing of GIS retreat from the shelf edge (Ó Cofaigh et al., 2013a, 2013b). The distribution of Paleozoic carbonate bedrock, mapped ice margin positions in northern Baffin Bay (Li et al., 2011) and central West Greenland (Ó Cofaigh et al., 2013a) and major ice streams are shown. UIS = Uummannaq ice stream; DIS = Disko ice stream; SSIS = Smith Sound ice stream; LSIS = Lancaster Sound ice stream. Northward-flowing West Greenland Current (WGC) is shown by the thin red line and the southward flowing Baffin Current (BC) is shown as a thin blue line. Inset shows temperature and salinity profile, 2008029-011CTD at the site of 2008029-12PC. http://geoscan.nrcan.gc.ca/starweb/geoscan/servlet.starweb?path=geoscan/downloade.web&search1=R=261330. (For interpretation of the references to color in this figure legend, the reader is referred to the web version of this article.)

the first-year ice formed in Baffin Bay (Buch et al., 2004), usually begins to form in September, expands from north to south, and reaches a maximum extent in March. It forms on the relatively fresh, cold ASW that enters from the Canadian Archipelago, and occupies the upper 100–300 m of the water column (Fig. 1). A second source of sea ice, the 'Stor-isen', travels into the area around SW Greenland with Polar Water of the EGC (Buch et al., 2004).

The connection between Baffin Bay and the Arctic Ocean was blocked by confluent Greenland, Innuitian and Laurentide ice sheets until the early Holocene (England et al., 2006; Zreda et al., 1999; Jennings et al., 2011), thus preventing the flow of ASW into Baffin Bay. Poor carbonate preservation in Baffin Bay by at least 5 cal ka BP (cf. Andrews and Eberl, 2011) is attributed to the inflow of carbonate under-saturated Arctic Surface Water (Azetsu-Scott et al., 2010) after deglaciation of the channels at the head of Baffin Bay (Jennings et al., 2011). In contrast, calcareous faunas are well preserved on the west Greenland Shelf under the influence of Atlantic water carried in the WGC (e.g. Perner et al., 2012).

3. Materials and methods

During two research cruises to Baffin Bay, we acquired sediment cores from the upper parts of the Disko and Uummannaq TMFs.

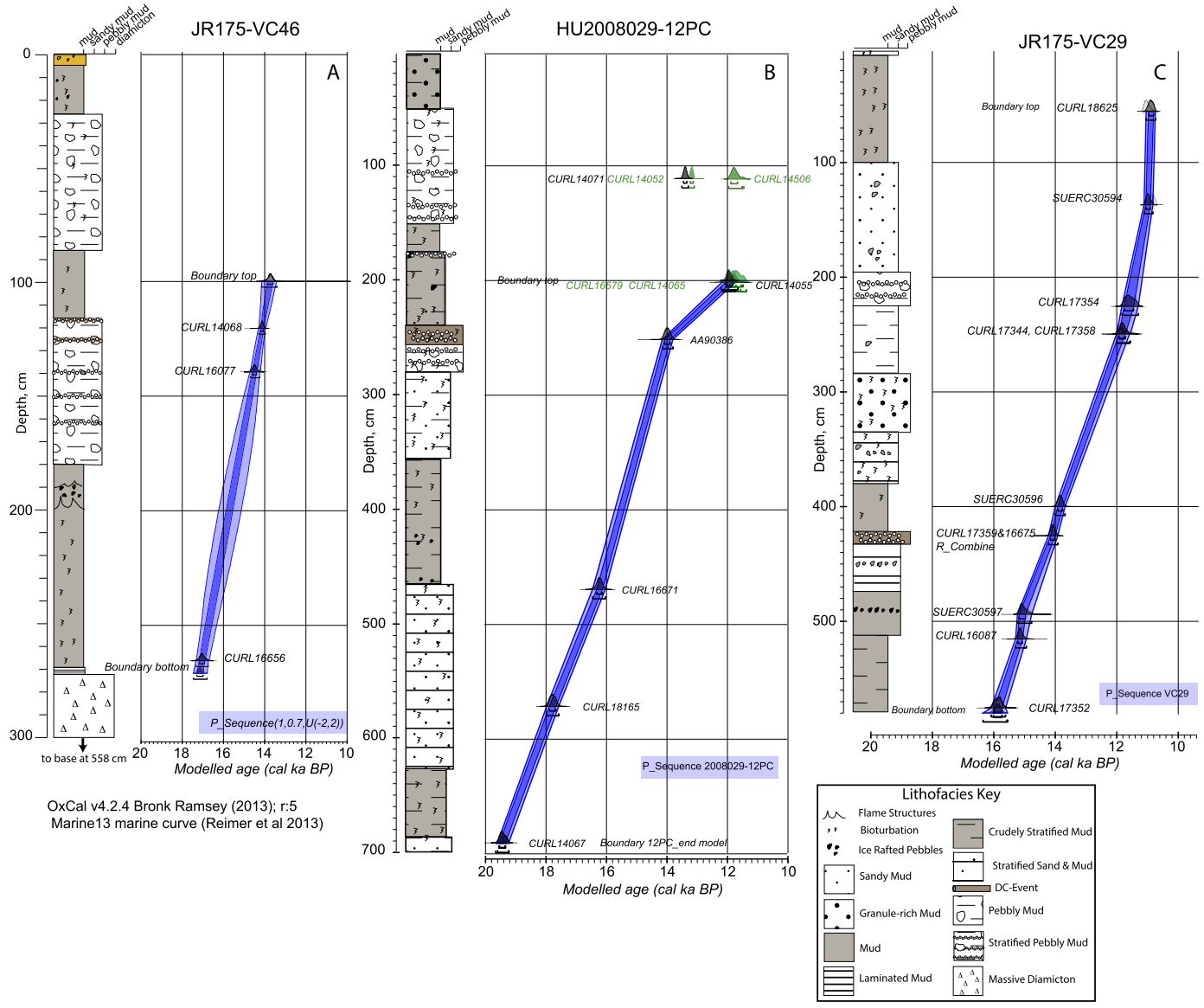

Fig. 2. Lithological logs against age-depth models for the three cores of this study. Dark blue and light blue shading denote 1σ and 2σ uncertainties of the model in each core. A. JR175-VC46. We exclude the upper 1 m from our age-depth model because the upper part of the core is undated. B. 2008-29-12PC. Note that benthic foraminiferal ages (green distributions) are not included in the age model; outliers at 1 m are excluded. C. JR175-VC29. The upper 55 cm of data are excluded because it is undated. Modeled age distributions are plotted for each dated sample (Table 1). (For interpretation of the references to color in this figure legend, the reader is referred to the web version of this article.)

The cores investigated in the current study are HU2008029-12PC (68°13.69′N; 57°37.08′W; 1475 m water depth), collected in 2008 from the Canadian vessel CSGS Hudson, together with JR175-VC29 (68°07.35′N; 59°44.36′W; 1064 m water depth) and JR175-VC46 (70°28.13′N; 61°2.91′W; 845 m water depth) collected in 2009 from the UK vessel RRS James Clark Ross (Fig. 1).

Core chronologies are based on radiocarbon (^{14}C) dates on planktonic and benthic foraminifera and mollusks (Fig. 2; Table 1). ^{14}C dates were calibrated using the Marine13 curve (Reimer et al., 2013). OxCal version 4.2.4 (Ramsey and Lee, 2013) was used to compute age/depth models and age uncertainties. We assume a marine reservoir offset (ΔR) of 140 ± 30 yrs based on recent work in Disko Bugt (Lloyd et al., 2011) and to align with recently published West Greenland core chronologies (cf. Jennings et al., 2014; Hogan et al., 2016; Sheldon et al., 2016). ΔR was likely larger in the LGM, but its magnitude and variation through time are unknown. Simon et al. (2012) support a ΔR range of 0–400 yrs in central Baffin Bay, which encompasses the ΔR value we have used.

To reconstruct the timing and environmental conditions of ice retreat, we have established basic lithofacies divisions for each core based on the sedimentary structures seen in x-radiographs and x-ray computed tomography (CT) scans (Fig. 2). We measured a series of climate/environmental proxies on each core and placed these into the context of the lithofacies changes. Our proxy data include counts of >2 mm clasts from x-radiographs (VC46 and VC29), and CT scans (12PC) of split cores as a measure of variations in ice-rafted debris (IRD) (Grobe, 1987). High counts of IRD are interpreted to reflect increased mass loss from the ice sheet by calving or as evidence of enhanced iceberg melt.

We distinguished the relative proportions of two major sediment sources, ‘distal’ northern Baffin Bay and ‘local’ CWG, to the TMFs using statistical analysis of quantitative x-ray diffraction mineralogy (qXRD) and the application of a sediment unmixing model applied to mineralogical analysis of a suite of Baffin Bay

Table 1
Details concerning the radiocarbon dates from the 3 cores of this study and their calibrated one sigma ranges, means and standard deviations as well as median values. Gray highlighted rows show ages excluded from the age models.

Core name	Reported age	Reported uncertainty	Radiocarbon Lab	Radiocarbon Lab number	$\delta^{13}C$	Depth, (cm)	Material dated	Sample weight (mg)	Calibrated ages, unmodeled (BP)								
									1 sigma			2 sigma					
									from	to	%	from	to	%	μ	σ	m
JR175-VC46	12770	30	CURL	14068	−0.3	120–121	*Cassidulina neoteretis*	4.5	14187	14045	68.2	14276	13961	95.5	14121	78	14118
JR175-VC46	12930	40	CURL	16077	3.1	139–140	Echinoid spines	7.6	14600	14236	68.2	14776	14141	95.5	14450	172	14435
JR175-VC46	14570	60	CURL	16656	4.7	262–267	NPS	2.3	17174	16915	68.2	17328	16749	95.5	17035	137	17070
HU2008029-012PC	11955	40	CURL	14071	5.8	110–112	NPS	2.3	13453	13344	68.2	13509	13295	95.4	13401	54	13400
HU2008029-012PC	10760	35	CURL	14065	4.8	201–202	NPS	1.2	12037	11845	68.2	12155	11715	95.4	11935	101	11942
HU2008029-012PC	12666	61	AA	90386	0.4	251–252	NPS	8.3	14100	13920	68.2	14177	13826	95.4	14007	88	13976
HU2008029-012PC	14030	40	CURL	16671	−1	469–470	NPS	6.6	16320	16133	68.2	16450	16033	95.4	16233	98	16225
HU2008029-012PC	15150	60	CURL	18165	−0.6	571–572	NPS	4.8	17891	17681	68.2	17980	17586	95.4	17784	100	17771
HU2008029-012PC	16660	45	CURL	14067	1	690–691	NPS	8.4	19555	19360	68.2	19619	19246	95.4	19446	76	19308
HU2008029-012PC	16600	50	CURL	16663	−1.1	780–781	NPS	5.5	19485	19275	68.2	19570	19187	95.4	19378	75	19500
HU2008029-012PC	18540	80	CURL	18628	0.2	859–860	NPS	5	21920	21661	68.2	22070	21525	95.4	21795	131	21758
HU2008029-012PC	11690	30	CURL	14052	2.1	110–112	*Cassidulina neoteretis*	3.9	13233	13132	68.2	13284	13095	95.4	13186	49	13185
HU2008029-012PC	10525	30	CURL	14506	−0.1	111–112	*Cassidulina neoteretis*	4.5	11890	11666	68.2	11963	11459	95.4	11749	123	11767
HU2008029-012PC	10490	40	CURL	16679	0.2	201–202	*Cassidulina neoteretis*	5.2	11829	11479	68.2	11904	11374	95.4	11653	142	11667
HU2008029-012PC	10540	25	CURL	14055	−1.3	201–202	*Cassidulina neoteretis*	5.4	11909	11720	68.2	11994	11568	95.4	11792	106	11804
JR175-VC29	10160	40	CURL	18625	4	54–57	Mixed benthic species	82	11115	10941	68.2	11160	10820	95.4	11006	88	11018
JR175-VC29	10057	39	SUERC	30594	−7	137	Paired bivalve	101.8	10975	10774	68.2	11058	10706	95.4	10880	93	10878
JR175-VC29	10570	40	CURL	17354	0.1	225–226	Mixed benthic species	4.4	11675	11370	68.2	11807	11281	95.4	11542	142	11538
JR175-VC29	10690	40	CURL	17344	−0.9	249–250	2 small gastropods	5.5	11962	11700	68.2	12025	11456	95.4	11788	143	11809
JR175-VC29	10710	35	CURL	17358	0.3	249–251	*Cassidulina neoteretis*	5.5	11980	11758	68.2	12065	11552	95.4	11837	125	11853
JR175-VC29	12494	41	SUERC	30596	0.3	400	Paired bivalve	4.1	13906	13753	68.2	13990	13674	95.4	13831	78	13830
JR175-VC29	12805*	50	CURL	17359	0.3	424–427	*Cassidulina neoteretis*	5.3	14132	13978	68.2	14205	13885	95.4	14052	80	14053
JR175-VC29	12710*	45	CURL	16675	−2.6	425–426	NPS	3.1	14269	14055	68.2	14512	13965	95.4	14200	135	14176
JR175-VC29	13194	63	SUERC	30597	−1.2	494	Paired bivalve	3.7	15189	14905	68.2	15275	14712	95.4	15011	151	15035
JR175-VC29	13255	40	CURL	16087	3.3	515–516	NPS	3.6	15238	15070	68.2	15313	14917	95.4	15134	96	15145
JR175-VC29	13760	60	CURL	17352	0.1	574–577	NPS	4.1	16000	15771	68.2	16111	15662	95.4	15884	114	15884

* Mean of 2 dates used in age model outliers or dates not used in age model.

Table 2
Benthic foraminiferal environmental preferences.

Species	Atlantic water	Arctic	Productivity	Glacial meltwater	Seasonal sea ice cover	Sea ice cover, low productivity	Strong currents	References
Calcareous species								
Astrononion gallowayi							X	Polyak et al., 2002
Buccella frigida	X		X		X			Polyak and Solheim, 1994; Steinsund, 1994
Cassidulina neoteretis	X				X			Jennings and Helgadottir, 1994; Seidenkrantz, 1995
Cassidulina reniforme	X			X	X			Hald and Korsun, 1997; Slubowska et al., 2005
Cibicides lobatulus							X	Wollenburg and Mackensen, 1998; Korsun and Polyak, 1989
Elphidium excavatum f. clavata		X		X				Hald and Korsun, 1997; Jennings and Helgadottir, 1994
Epistominella arctica		X				X		Wollenburg and Mackensen, 1998
Islandiella helenae		X	X		X			Wollenburg et al., 2004
Islandiella norcrossi	X				X			Lloyd, 2006; Steinsund, 1994
Melonis barleeanus	X		X		X			Caralp, 1989; Corliss, 1991; Jennings et al., 2004; Wollenburg and Mackensen, 1998
Nonionella turgida	X		X		X			Wollenburg et al., 2004; Jennings et al., 2004; Rytter et al., 2002
Nonionellina labradorica			X		X			Jennings et al., 2004; Polyak et al., 2002; Rytter et al., 2002
Pullenia bulloides	X							Wollenburg et al., 2004; Rytter et al., 2002
Stainforthia concava		X	X		X			Steinsund, 1994; Jennings and Helgadottir, 1994; Polyak et al., 2002
Stainforthia feylingi		X	X		X			Knudsen and Seidenkrantz, 1994; Seidenkrantz, 2013
Stetsonia horvathi		X				X		Wollenburg and Mackensen, 1998
Agglutinated species								
Cuneata arctica		X						Schafer and Cole, 1988; Lloyd, 2006
Portatrochammina bipolaris		X						Jennings and Helgadottir, 1994; Schröder-Adams et al., 1990
Reophax catella	X							Höglund, 1947
Reophax catenata	X							Höglund, 1947
Reophax subfusiformis	X							Lloyd, 2006 (as *R. fusiformis*)
Saccammina difflugiformis	X							Schafer and Cole, 1988; Scott and Vilks, 1991
Spiroplectammina biformis		X		X				Jennings and Helgadottir, 1994; Schafer and Cole, 1986
Textularia earlandi	X	X						Jennings and Helgadottir, 1994; Schafer and Cole, 1986; Lloyd, 2006

surface sediments (see Andrews and Eberl, 2011, 2012). Changes in sediment provenance indicate whether hemipelagic sediments on the TMFs were supplied by 'local' Disko and Uummannaq ice streams, and potentially sediments from other West Greenland outlets, or by distal Laurentide, Innuitian and north GIS ice margins terminating in northern Baffin Bay (NBB) (Li et al., 2011; England et al., 2006) (Fig. 1). The provenance data are reported as sediment source fractions attributed to NBB vs. CWG (Supp. Fig. 1). The mineralogy of the CWG ice streams is distinct from central Baffin Bay (Simon et al., 2014) and the Davis Strait (Andrews et al., 2014). The most obvious signal of NBB glacier margin input is detrital carbonate including dolomite and calcite eroded from Paleozoic carbonate bedrock, and the NBB source as reconstructed herein is closely tied to its occurrence (Andrews and Eberl, 2011) (Fig. 1; Supp. Fig. 1).

Benthic and planktonic foraminiferal assemblages were quantified and Principal Component Analysis (PCA) of the benthic assemblages of each core was run separately, providing a set of principal component axes for each core. Known environmental associations of the most important benthic species on the PCA axes from each core were then used to interpret changes in the presence of relatively warm Atlantic Water as a subsurface water mass (AIW), glacial meltwater production, water-column stratification with cold/sea-ice covered surface waters, and onset of the WGC at the core sites (Table 2; Fig. 3).

Stable isotope data on the planktic foraminifer *Neogloboquadrina pachyderma* sinistral (NPS) acquired from VC29 are used to test for isotopically light glacial meltwater during deglaciation. The biomarker IP_{25} (Belt et al., 2007) was quantified in 12PC only, to assess for the presence of seasonal sea ice. Descriptions of all proxy methods are in the Supplemental Information.

4. Background and previous work

Evidence on the extent of the GIS at the LGM has grown in recent years but is still sparse for many areas (Funder et al., 2011; Vasskog et al., 2015). Geophysical data collected in 2009 showed that grounded ice extended across the CWG margin through the Uummannaq and Disko troughs as fast flowing ice streams (Ó Cofaigh et al., 2013a, 2013b; Dowdeswell et al., 2014). Debris flows and turbidites on the Disko and Uummannaq TMFs also provide evidence for an ice sheet margin grounded at the shelf edge (Ó Cofaigh et al., 2013a, 2013b). A minimum estimate of the timing of ice retreat from the outer Uummannaq trough is provided by a ^{14}C date of 15 cal ka BP in glacial marine sediments overlying till on the shelf (O´ Cofaigh et al., 2013b; Sheldon et al., 2016). Sheldon et al. (2016) proposed that a large grounding zone wedge in the outer-middle reaches of the Uummannaq Trough marks a stable ice position during the Younger Dryas (YD) and that the Uummannaq Ice Stream retreated episodically from its LGM shelf edge position.

The timing of LGM retreat from the Disko Trough shelf edge is not well constrained due to a YD re-advance of the ice stream; however, an estimate of ice retreat from the LGM position c. 13.8 cal ka BP is based on ^{14}C dates on shells entrained in sediment gravity flows in cores from the Disko TMF (Ó Cofaigh et al., 2013b). New 3D-seismic mapping of the banks adjacent to Disko Trough suggests that grounded ice retreated in phases from the LGM position and that the GIS grounded on the middle shelf banks during the YD (Hofmann et al., 2016b). Hogan et al. (2016) showed that the ice margin stabilized on an inner shelf bathymetric high c. 12.1 cal ka BP (Hogan et al., 2016). YD ice retreat in CWG is marked by increased IRD flux (Jennings et al., 2014;

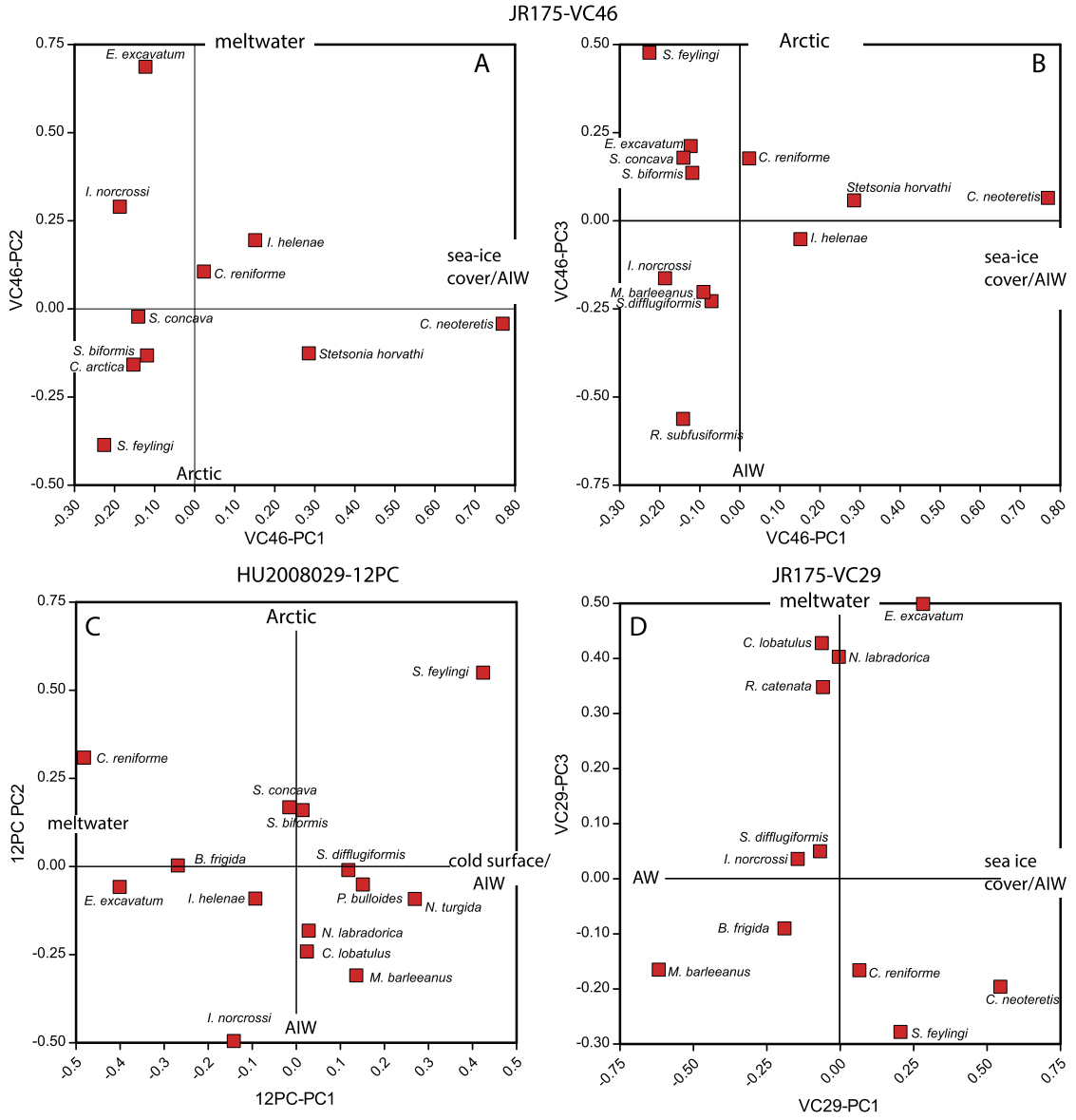

Fig. 3. PCA scores of significant species on PCA axes of the 3 cores and their environmental interpretations. A and B: JR175-VC46 species scores on the first 3 PCA axes. C: 2008029-12PC, species scores on PCA axes 1 and 2. D: JR175-VC29 species scores on PCA axes 1 and 3. See Supp. Table 1 for full list of species scores.

Sheldon et al., 2016) consistent with rapid ice retreat into the fjords (Lane et al., 2014; Roberts et al., 2013; Hogan et al., 2011).

Knutz et al. (2011) proposed a model of ice retreat for southern Greenland in which the initial retreat from the shelf edge was promoted by subsurface Atlantic Water from the IC. The ensuing rapid mass loss by calving produced pulses of ice rafted clasts (IRD) between the LGM and the early Holocene with predominantly Greenland provenance signatures (Knutz et al., 2013). Offshore of CWG, the WGC was established by 14 cal ka BP in association with strong melting of icebergs from Northern Baffin Bay and West Greenland ice margins (Sheldon et al., 2016). NBB icebergs melted preferentially along the CWG slope and outer shelf through contact with the warm WGC thus forming a conspicuous detrital carbonate-rich layer, or DC event (Sheldon et al., 2016), that is at least partly correlative with a marker of ice margin instability of northern Baffin Bay ice streams, Baffin Bay Detrital Carbonate event 1 (BBDC1) (15–13.7 cal ka BP) (Andrews et al., 1998; Simon et al., 2014). A younger BBDC event in the Disko Trough from 11.6 to 10.6 cal ka BP (Jennings et al., 2014), correlates with the youngest BBDC event in Baffin Bay (Simon et al., 2014) and with detrital carbonate events noted on the Baffin Island shelf (Andrews et al., 1996) and central Davis Strait (Knutz et al., 2013).

5. Results presented on each core from North to South

5.1. JR175-VC46 (VC46), Uummannaq TMF

The benthic foraminiferal faunal variations are summarized by the first 3 PC axes (Figs. 3A, B; 4B, C, E; Supp. Info Table 1; Supp. Fig. 2). VC46-PC1 explains 21.64% of the variance in the assemblages. VC46-PC1 has positive scores on species found in oligotrophic (*Stetsonia horvathi*) and pulsed productivity (*Islandiella helenae*) conditions associated with sea-ice cover and AIW (*C. neoteretis*) (Fig. 3A, B) (Jennings and Helgadottir, 1994 Wollenburg and Mackensen, 1998; Wollenburg et al., 2004) (Table 2). Positive loadings on VC46-PC1 are interpreted to represent water-column stratification with cold, sea-ice bearing surface waters with a warmer subsurface AIW layer.

VC46-PC2 explains 14.2% of the variance in VC46 assemblages and is positively associated with *E. excavatum* f. *clavata*, an opportunistic species capable of withstanding unstable environmental

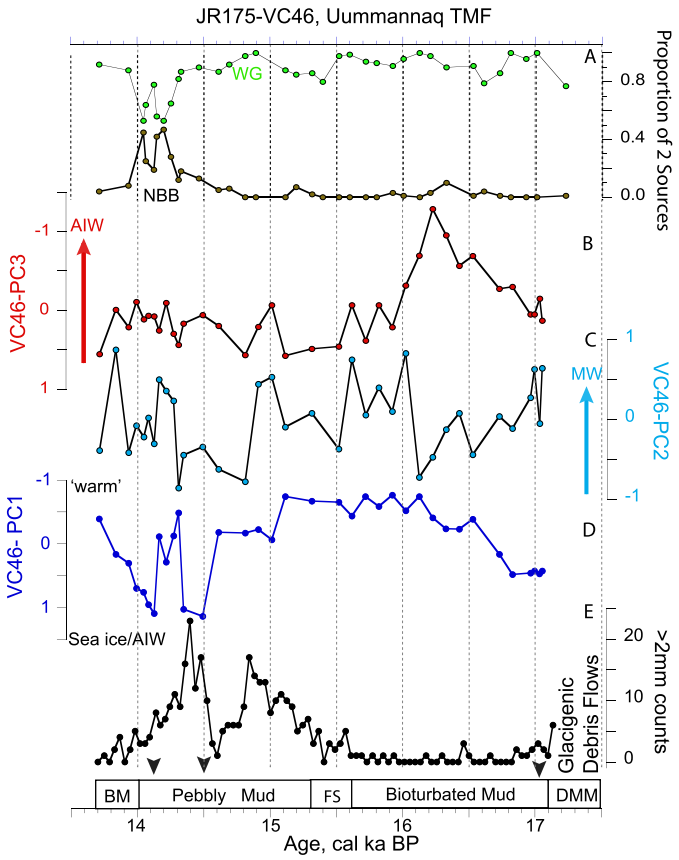

Fig. 4. Proxy data and lithofacies against calibrated age from JR175-VC46, Uummannaq trough mouth fan. A. Proportion of sediment from northern Baffin Bay (brown) and the CWG (green). B, C, D. Foraminiferal PCA loadings on axes 1, 2, 3, respectively. E. Counts of >2 mm grains attributed to iceberg rafting. Triangles on the *x*-axis show locations of radiocarbon dates. Lithofacies: BM = bioturbated mud; FS = flame structures; DMM = matrix supported diamicton. (For interpretation of the references to color in this figure legend, the reader is referred to the web version of this article.)

conditions and turbid glacial meltwater (cf. Hald and Korsun, 1997) (Table 2; Fig. 3A). Positive loadings on PC Axis 2 are associated with unstable conditions and presence of turbid glacial meltwater (Fig. 3A).

VC46-PC3 explains 11.8% of the variance in VC46 assemblages. Axis 3 has negative species scores on Atlantic Water indicator species including: *Melonis barleeanus*, *Islandiella norcrossi*, *Saccammina difflugiformis* and *Reophax subfusiformis* (Table 2). Significant positive species scores are on *Stainforthia feylingi*, an arctic species indicative of cold, low salinity surface waters (Lloyd, 2006) and seasonal sea ice formation (Seidenkrantz, 2013). Negative sample scores on VC46-PC3 were interpreted to indicate the presence of relatively warm AIW, below, or at, the grounding line of the glaciers (Fig. 3B).

The chronology of VC46 is constrained by 3 radiocarbon dates (Fig. 2A). One-sigma errors on the downcore age estimates range between 80 and 240 yrs. Matrix-supported, massive diamicton, interpreted as glacigenic debris flows (GDFs) by Ó Cofaigh et al. (2013a) occur from the base of the core (558 cm) to 270 cm. The GDFs record downslope sedimentation in front of the Uummannaq ice stream during the LGM when it was grounded at the shelf edge (Ó Cofaigh et al., 2013a). GDF mineral composition is dominated by the Greenland source but has a minor component from northern Baffin Bay (Ó Cofaigh et al., 2013a) (Fig. 4A).

A unit of fine-grained bioturbated mud with a primarily West Greenland sediment source and with rare or absent >2 mm clasts (IRD) overlies the GDFs from 270–180 cm (17.1–15.3 cal ka BP) (Fig. 2A). A date on NPS from 262–267 cm constrains the timing of the transition from GDFs into the overlying mud to 17.1 cal ka BP. At its top (198–180 cm; 15.6–15.3 cal ka BP), the mud contains flame structures and a slight increase in IRD suggesting rapid episodic deposition (Fig. 2A, Fig. 4A, E). The sediments in this interval continue to be dominated by the Greenlandic source (0.8–1.0), although the NBB source is present (up to 0.1) (Fig. 4A).

A transition to pebbly mud begins at 180 cm (15.3 cal ka BP) and extends to 115 cm (14 cal ka BP) (Fig. 2A). Within this, the IRD displays two large peaks (Fig. 4E). The first peak, from 180–146 cm (15.3–14.7 cal ka BP) comprises sediments derived primarily from CWG sources (Fig. 4A). The second peak, from 141–115 cm (14.5–14 cal ka BP), contains a distinct rise in detrital carbonate from 14.3–14 cal ka BP (Fig. 4A, E) indicative of an increased sediment contribution from northern Baffin Bay (Fig. 4A). The NBB DC event is overlain by bioturbated mud with low IRD (Fig. 4E). A second interval of pebbly mud from 85–25 cm is overlain by bioturbated mud. These units postdate the uppermost radiocarbon age of 14.12 ± 0.08 cal ka BP at 120 cm (Fig. 2A).

The VC46 record begins with positive loadings on VC46-PC1 and 2 indicating cold conditions associated with glacial meltwater and sea-ice cover between 17 and 16.9 cal ka BP, immediately after cessation of GDF deposition (Fig. 4C, D). A progressive, warming signal is recorded by increasingly negative loadings on VC46-PC3 (16.9 to 16.2 cal ka BP) (Fig. 4B). This subsurface warm interval occurs within the bioturbated mud overlying the GDFs. From 16.1 to 14.9 cal ka BP high positive loadings on VC46-PC2 indicate glacial meltwater in the upper part of the bioturbated mud and the lower unit of pebbly mud (Fig. 4C). The meltwater signal declines after 14.9 cal ka BP, shortly before the end of the IRD-rich pebbly mud with Greenlandic source (Fig. 4A, C, E).

The upper IRD-rich interval between 14.5 and 14.0 cal ka BP is an NBB DC event characterized by distinct shifts between VC46 PCA Axes 1 and 2, reflecting shifts in cold, sea-ice covered conditions and glacial meltwater. The interval 14.5–14.0 cal ka BP has positive VC46-PC1 loadings separated by a brief interval of positive loadings on VC46-PC2 and strongly negative loadings on VC46-PC1. This pattern suggests that the NBB DC event begins with a stratified water column, with cold, sea-ice covered waters overlying submerged Atlantic Water (AIW) (14.5–14.3 cal ka BP). The environment shifts briefly to relatively warmer conditions associated with glacial meltwater production (14.3–14.2 cal ka BP) and then returns to cold sea surface with AIW conditions between 14.2 and 14 cal ka BP. The top of the dated record, coinciding with bioturbated mud, shows a warming trend with increasing meltwater.

5.2. HU2008029-12PC (12PC) Northern Disko TMF

The first two PCA axes capture 44% of the variance in the benthic foraminiferal assemblages (Fig. 3C). *S. feylingi* had significant positive scores on 12PC-PC1 (27.2% of variance). This species is dominant under conditions of a cold freshwater lid and associated sea-ice edge productivity (Seidenkrantz, 2013; Lloyd, 2006). The glacial marine species *E. excavatum* and *C. reniforme* have negative scores on VC46-PC1. These species are indicative of conditions warm enough to generate glacial meltwater.

12PC-PC2 (17.4% variance) is represented by negative scores of *M. barleeanus, I. norcrossi, Buccella frigida and Nonionellina labradorica*. These species are consistent with nutrient rich Atlantic Water. Negative sample scores on 12PC-PC2 are interpreted to indicate the presence of AIW, below or at the grounding line of the glaciers, and thus very similar to the VC46-PC3 (Fig. 3B, C).

Core 12PC extends well into the LGM, but for the purposes of comparison with VC46 and VC29, we limit the discussion of data to ≤17.5 cal ka BP (554 cm). An age reversal at 1 m limits the chronology to depths of ≥200 cm (11.9 cal ka BP). The 12PC age

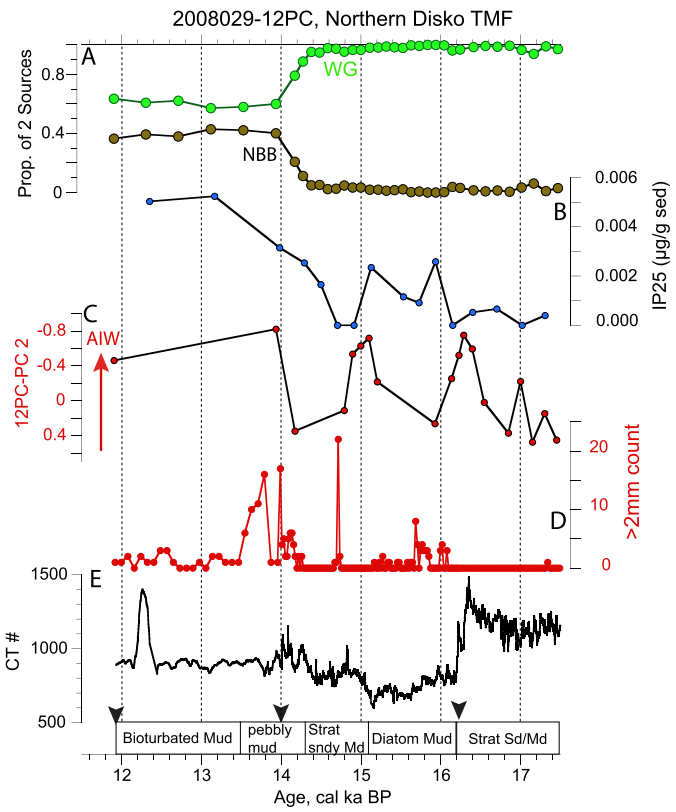

Fig. 5. Proxy data and lithofacies against calibrated age from 2008029-12 PC, northern Disko trough mouth fan. A. Proportion of sediment from northern Baffin Bay (brown) and central West Greenland (green). B. IP_{25} data. C. Sample loadings on PCA axis 2 where higher negative loadings indicate increased submerged Atlantic Water influence. D. Counts of >2 mm clasts from the CT images. E. CT number and the positions of radiocarbon ages that constrain this part of the chronology (black arrowheads). Lithofacies: Strat Sndy Md = stratified sandy mud; Strat Sd/Md = Stratified sand and mud.

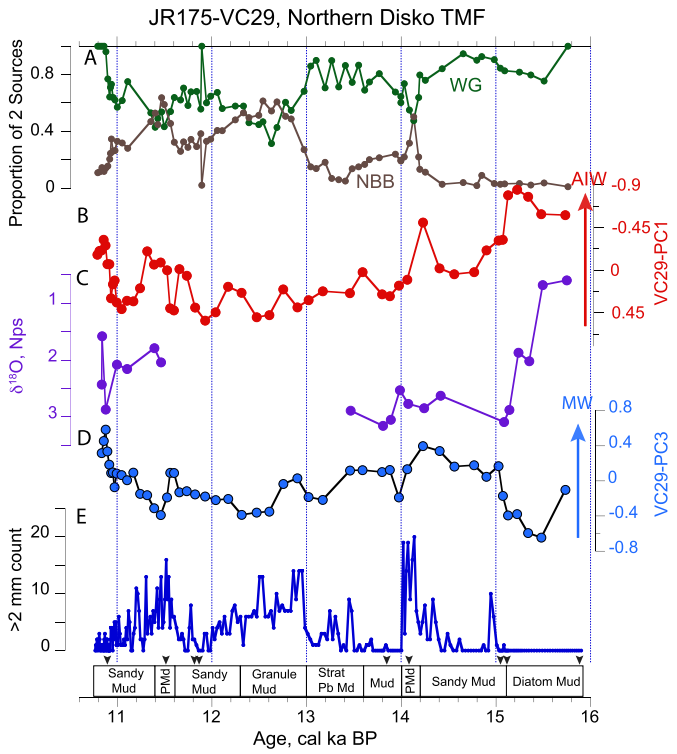

Fig. 6. Proxy data and lithofacies against calibrated age from JR175-VC29, northern Disko trough mouth fan. A. Proportion of sediment from northern Baffin Bay (brown) and central West Greenland (green). B. Foraminiferal PCA loadings on axes 1. C. $\delta^{18}O$ values from *Neogloboquadrina pachyderma* sinistral. D. foraminiferal PCA loadings on axis 3. E. Counts of >2 mm grains attributed to iceberg rafting. Triangles on the *x*-axis show locations of radiocarbon dates. Lithofacies: PMd = Pebbly mud; Strat Pb Md = stratified pebbly mud. (For interpretation of the references to color in this figure legend, the reader is referred to the web version of this article.)

model is based upon 5 radiocarbon dates from 201–691 cm on the arctic planktonic foraminifer, NPS (Fig. 2B; Table 1). One-sigma errors on the downcore age estimates are ±100 yrs.

The CT number (CT#), a measure of sediment density, marks shifts in sand content from high sand/high density to low sand/low density in the core (Fig. 5E). A high CT# interval of bioturbated, stratified sand and mud from >17.5 cal ka BP (554 cm) to 16.2 cal ka BP (467 cm) is overlain by much finer, crudely stratified mud with low CT# that extends to 15.1 cal ka BP (356 cm) (Fig. 2B; Fig. 5E). The mud is dominated by siliceous microfossils (centric diatoms and *Chaetoceras* setae), and has rare IRD near its base (Fig. 2B, Fig. 5D). The radiocarbon age from 469–470 cm closely constrains the timing of the transition between these units to 16.2 ± 0.1 cal ka BP.

A prominent peak of negative 12PC-PC2 loadings begins prior to the transition and ends soon after, indicating the presence of relatively warm ocean waters at intermediate depths by 16.6 cal ka BP (Fig. 5C; Supp. Fig. 2). The presence of the biomarker IP_{25} indicates the occurrence of seasonal sea ice between 16.2 and 15.1 cal ka BP (Fig. 5B), and the high diatom content of the sand fraction supports that this is also an interval of increased marine productivity, although foraminifera were too sparse for PCA analysis. Sand content, stratification and bioturbation increase at 15.1 cal ka BP (356 cm) (Fig. 5E), coinciding with another peak from 15.1 to 14.9 cal ka BP in negative loadings on 12PC-PC2 indicating warm subsurface water (Fig. 5C), but a fall in IP_{25} content (Fig. 5B). At 14.3 cal ka BP (280 cm) coarse dispersed IRD and sand layers become pronounced (Fig. 2B; Fig. 5D, E), coinciding with the shift from Greenland sediment provenance to a mixed NBB (0.4) and Greenland (0.6) sediment provenance, and marking an NBB DC event beginning at 14.3 cal ka BP (Fig. 5A). This transition is preceded by a major rise in IP_{25} (Fig. 5B) and a strongly negative 12PC-PC2 loading (Fig. 5C), suggesting a shift to more consistent seasonal sea ice formation by 14.3 cal ka BP.

5.3. JR175-VC29, Northern Disko TMF

The first three PCA axes explain 47.8% of the variance in the benthic foraminiferal data (Fig. 3; Supp. Fig. 4). VC29-PC1 (19.4%) was associated with positive scores on water column stratification indicators, *C. neoteretis* and *S. feylingi* and negative scores on Atlantic Water indicators *Melonis barleeanus*, *B. frigida*, and *I. norcrossi* (Fig. 3D; Table 2). Negative loadings on VC29-PC1 are interpreted to express AIW similar to VC46-PC3 and 12PC-PC2. VC29-PC2, accounting for 17.2% of the variance separated agglutinated from calcareous dominated assemblages and is not interpreted further. VC29-PC3, accounting for 11.2% of the variance, was associated with significant positive scores of glacial marine species *E. excavatum* f. *clavata* reflecting Greenland sourced turbid meltwater, as seen for VC46-PC2 and 12PC-PC2 (Fig. 3).

The VC29 chronology is based on 10 calibrated radiocarbon dates (Table 1; Fig. 2C) and spans the interval 15.9 to 10.8 cal ka BP. One-sigma errors on the downcore age estimates range between 70 and 400 yrs (Fig. 2C).

Fine-grained, crudely stratified mud of Greenlandic provenance and rich in sand-sized diatoms extends from 590 to 512 cm (15.9–15.1 cal ka BP) (Fig. 6A, Fig. 2C). This unit has the highest negative loadings on VC29-PC1, indicating relatively warm subsurface conditions, especially from 15.9 to 15.2 cal ka BP (Fig. 6B). NPS occurs in high numbers (up to 200/g) coinciding with spikes

in the benthic foraminiferal abundances (Supp. Fig. 4) and records very light $\delta^{18}O$ values (2–0.7‰) indicating cold low salinity surface water (Fig. 6C) or rapid sea ice formation (Hillaire-Marcel and de Vernal, 2008). This unit is similar in timing and diatom content to the fine grained, diatom-rich mud above the transition in 12PC (Fig. 5).

From 512–419 cm (15.1–14.0 cal ka BP) the sediments become sandy and well stratified with progressively increasing IRD content, and ending with a pronounced increase in IRD from 433–419 cm (14.2–14.0 cal ka BP) (Fig. 2C; Fig. 6E). By 15.1 cal ka BP the loadings on VC29-PC1 trend toward positive values while loadings on VC29-PC3 rise, suggesting increased glacial meltwater (Fig. 6B, D). This lithofacies has Greenlandic provenance until the peak IRD interval (14.2–14 cal ka BP), which coincides with a peak in NBB provenance up to 0.5 (Fig. 4A). VC29-PC1 becomes more positive overall in this interval, recording ocean cooling, except for a peak from 14.4–14.2 cal ka BP that records a brief reversal to warmer ocean conditions immediately prior to the IRD/NBB peak (Fig. 6A, B). This negative peak in VC29-PC1 loadings is associated with abundant *Cassidulina neoteretis* a species commonly associated with AIW around Greenland (Table 2; Supp. Fig. 4) although absent in the >90% agglutinated faunas (Sheldon, personal Communication) that occur today on the West Greenland slope due to carbonate dissolution in Baffin Bay (Azetsu-Scott et al., 2010).

Between 419 and 282 cm (14–12.3 cal ka BP) there is a similar sequence of lithofacies and provenance to the sequence below. The sequence begins with mud with mixed NBB and Greenland provenance from 419–380 cm (14–13.6 cal ka BP). Between 380 and 334 cm (13.6–13 cal ka BP) the sediments change to stratified pebbly mud of Greenlandic provenance (Fig. 6A, E). Steadily increasing loadings on VC29-PC1 indicate cooling (Fig. 6B). Positive loadings on VC29-PC3 change to negative loadings by 13 cal ka BP indicating declining meltwater input (Fig. 6D). At 13 cal ka BP (334 cm) the NBB source returns abruptly and is associated with a rise in coarse IRD (Fig. 6A, E). The NBB source continues to exceed the Greenland source until 12.3 cal ka BP. Over the full period from 14–12.3 cal ka BP, VC29-PC1 trends gradually toward more positive values indicating cooling ocean conditions (Fig. 6B) and planktic and benthic foraminifera per gram are low, suggesting low productivity (Supp. Fig. 4).

Between 282 and 225 cm (12.3–11.6 cal ka BP) the sediments are sandy, crudely stratified mud with rare IRD (Fig. 2C; Fig. 6E). This unit is dominated by the Greenlandic source but maintains a background of 0.3 to 0.4 of NBB sediments (Fig. 6A). A shift to greater faunal abundances (Supp. Fig. 4) and more negative VC29-PC1 loadings supports slightly warmer conditions and a rise in VC29-PC3 loadings suggests increased meltwater (Fig. 6B, D).

A final interval of stratified IRD rich sediment extends from 225–196 cm (11.6–11.4 cal ka BP) (Fig. 2C; Fig. 6E). High IRD is once again associated with a pronounced peak in NBB source up to 0.6 of the sediment (Fig. 6A). A dip in VC29-PC3 loadings and very brief positive excursion in VC29-PC1 loadings support a brief cooling and reduction in Greenlandic meltwater associated with this NBB/IRD peak (Fig. 6B, D). The light stable isotope values on NPS (Fig. 6D) and strong rise in percentages of *S. feylingi* (Supp. Fig. 5) indicate increased freshwater and icebergs from NBB.

Between 196 and 100 cm (11.4–10.9 cal ka BP) sediments are bioturbated sandy mud with diminishing >2 mm IRD (Fig. 2C; Fig. 6E). The NBB source declines (Fig. 6A) and by 11 cal ka BP, VC29-PC1 shifts to higher/warmer values (Fig. 6B). Loadings on VC29-PC3 increase steadily between 11.4 cal ka BP and 10.8 cal ka BP, indicating increased meltwater (Fig. 6D). Above 100 cm (10.9 cal ka BP), the sediments transition to bioturbated mud with rare IRD (Fig. 2C).

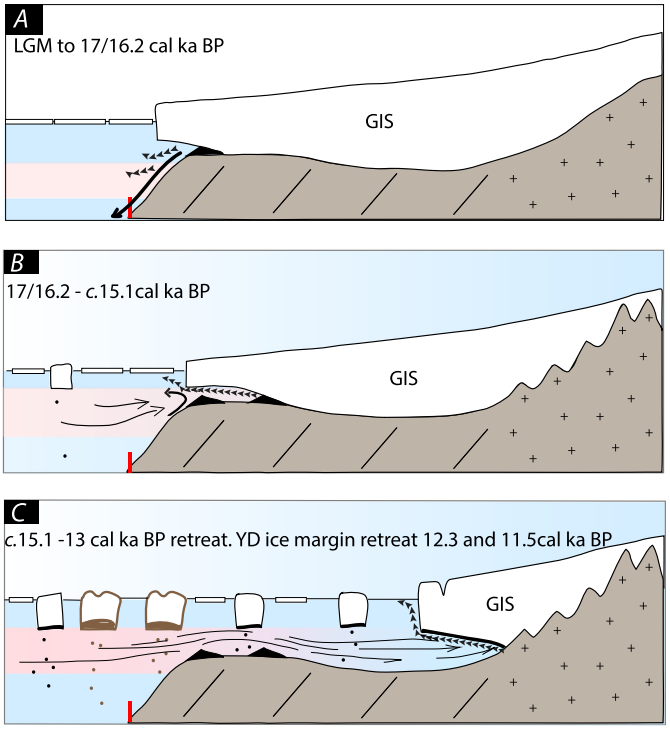

Fig. 7. Schematic illustrations summarizing the ice sheet ocean interactions in central west Greenland (modified from Knutz et al., 2011). Panel A illustrates the LGM position of the GIS outlets at the shelf edge with the ice margin feeding the trough mouth fans and heavy sea ice in Baffin Bay. Panel B illustrates the initial retreat of the ice from the shelf edge and retention of a buttressing ice shelf that filtered out coarse material at the grounding line, released fines to the slope, and produced small grounding zone wedges on the outer Uummannaq Trough. A slight reduction in buttressing sea ice is depicted. Panel C illustrates the calving retreat of the ice sheet as the grounding line retreat toward a reverse slope under the influence of warm ocean water. Red vertical bar denotes location of the 3 cores in the study. Brown-based icebergs and IRD denote a northern Baffin Bay (NBB) source whereas black-based icebergs denote a central West Greenland (CWG) source. The onset of a seasonal sea ice presence is depicted. (For interpretation of the references to color in this figure legend, the reader is referred to the web version of this article.)

6. Discussion

We discuss our results via two questions that deal with the fundamental glaciological and oceanographic changes in the location of the margin of the GIS in our study area.

6.1. When did the GIS grounding line first retreat from the shelf edge and was its retreat gradual, episodic or rapid?

Using the stratigraphic relations, proxy data interpretations, and calibrated dates of our three slope cores, we have built a conceptual model of grounding line retreat from the shelf edge in CWG (Fig. 7). Our model is based on an earlier schematic model (Knutz et al., 2011), but is developed further to reflect the new information on CWG glacial history derived from our study. Two of the cores, VC46 and 12PC, have dated sedimentary evidence marking Uummannaq and Disko ice stream retreat from the shelf edge, respectively (Fig. 7A). In VC46, the end of GDF deposition and onset of hemipelagic sedimentation at ca. 17.1 cal ka BP marks grounding-line retreat of the Uummannaq ice stream. In 12PC, the strong reduction in sediment density at 16.2 cal ka BP marks grounding-line retreat from the shelf edge of the Disko ice stream. In both cores constraining ages are close to this boundary, supporting at least a 400 yrs difference (at 2σ) in the timing of ice retreat between the Uummannaq and Disko ice streams. The deeper shelf edge in Uummannaq Trough (>600 m) compared to the much shallower shelf edge of the Disko Trough (350 to 400 m) may have

allowed earlier access of warm intermediate water to the Uummannaq ice stream grounding line, thereby assisting earlier retreat.

In all three cores, a fine-grained interval essentially barren of IRD occurs after ice retreat. The fine-grained unit extends to 15.1 cal ka BP in the case of the Disko TMF cores (VC29 and 12PC) and to ca. 15.3 cal ka BP in the case of VC4 (age-equivalent at 1σ) (Fig. 7B). Had the ice margins and grounding line retreated landward rapidly by calving, this unit would have contained IRD clasts >2 mm. Instead, we attribute the lack of IRD to signify retention of a buttressing ice shelf as the grounding line retreated slowly across the outer shelf (Fig. 7B). With an ice shelf, coarser-grained material would have been preferentially deposited proximal to the grounding line, leaving icebergs calved from the ice-shelf front relatively clean of debris (Domack and Harris, 1998). Prior evidence for this scenario comes from geophysical data from the outer Uummannaq trough where several small grounding zone wedges are defined on the landward shallowing outer shelf (Sheldon et al., 2016; their Fig. 2A), suggesting episodic retreat. At the same time, fine sediments would have been carried to the slope sites in turbid meltwater plumes emanating from the grounding line and by resuspension of fine materials by currents (Fig. 7B), resulting in the fine grained mud unit (Domack and Harris, 1998).

The rise in Greenlandic IRD by 15.3 cal ka BP in Uummannaq trough indicates loss of the fringing ice shelf and retreat of a predominantly grounded ice front by calving of debris-laden ice bergs (Fig. 7C). In VC29 and 12PC, ice retreat by calving commenced at 15.1 cal ka BP based on increasing sand content in 12PC and by the shift to stratified sand with IRD in VC29. The age-control is best in VC29, suggesting that 15.1 cal ka BP is the better age estimate of the onset of the calving event (Fig. 2C), although the rise in IRD is age-equivalent at 1σ in the three cores. IRD may also have been contributed by icebergs calved from outlet glaciers along the southwestern Greenland margin.

In VC46 there is a clear end to the contribution of Greenland IRD by 14.7 cal ka BP, with a lull in IRD contribution prior to the start of the second IRD peak at 14.5 cal ka BP, and a peak in NBB sourced IRD from 14.3–14.0 cal ka BP. The NBB IRD event began at 14.2 cal ka BP in VC29 and 12PC and ended by 14 cal ka BP; once again overlapping at 1σ. In VC29 and 12PC, there is no distinct gap separating the Greenland glacimarine sediments from the NBB IRD peak. An NBB event at 14 cal ka BP was also observed in JR175-VC45 on the outer Uummannaq Trough (Sheldon et al., 2016). The NBB West Greenland DC event essentially forms a marker horizon indicating an increase in drift of NBB icebergs to the CWG margin where they melted preferentially as they encountered warmer Atlantic Water. We infer that, prior to the early Holocene opening of the channels in the Canadian Arctic Archipelago, the Baffin Current may have been less vigorous, allowing Baffin Bay surface waters to spread within Baffin Bay such that NBB icebergs could reach West Greenland.

A second phase of Greenland IRD and stratified sand began by 13.6 cal ka BP in VC29 signifying renewed calving from the GIS, still grounded on the shelf. Once again, this Greenland IRD interval is capped by IRD input from the NBB source at 13 cal ka BP. The NBB event continued until 12.3 cal ka BP, when the provenance again became dominated by Greenland sources. Between 12.3 and 11.6 cal ka BP, the Greenland source was dominant and the sandy sediments likely record retreat of the Disko Ice Stream from its Younger Dryas position at the shelf edge (Ó Cofaigh et al., 2013b; Jennings et al., 2014). Between 11.6 and 11.4 cal ka BP there is a final NBB IRD event. A DC event of similar onset but longer duration (11.6 to 10.6 cal ka BP) was recorded in cores from the outer Disko Trough (Jennings et al., 2014). This final NBB event is followed by deposition of dominantly Greenlandic sediment with coarse IRD and sand that likely records ice retreat into Disko Bugt (Hogan et al., 2016), and, in Uummannaq Trough, rapid retreat from the large mid-shelf grounding-zone wedge (Sheldon et al., 2016).

The results indicate that the GIS continued to contribute glacigenic sediments from iceberg rafting and meltwater plumes to the TMFs until the early Holocene. This prolonged ice-stream sediment contribution to the fans supports other recent studies that infer the presence of ice streams in the shelf troughs until the early Holocene (Hogan et al., 2016; Sheldon et al., 2016). Our data also indicate that the ice sheet began to retreat c. 17.1 cal ka BP in the Uummannaq Trough and at c. 16.2 cal ka BP in the Disko Trough, coincident with gradual eustatic sea level rise associated with the main phase of deglaciation (Lambeck et al., 2014). However, we do not know the exact change in relative sea level (glacioisostatic and eustatic) and do not claim that sea-level rise was a driver of ice retreat. The initial timing of grounding line retreat from the shelf edge along CWG is therefore significantly earlier than 13.8 cal ka BP as inferred previously by Ó Cofaigh et al. (2013b) using data available at that time for the Disko ice stream, but older than the 15 cal ka BP age of ice retreat from the Uummannaq ice stream recorded from the outer Uummannaq trough (Sheldon et al., 2016; Dowdeswell et al., 2014). This key outcome demonstrates that the initial CWG ice retreat from the shelf edge was closer in timing to that of ice retreat in East Greenland of 18–17 cal ka BP, contrary to what was previously thought (Vaskogg et al., 2015; Ó Cofaigh et al., 2013b; Jennings et al., 2006; Evans et al., 2002).

6.2. Did ocean warming (Atlantic Water inflow) initiate and sustain retreat?

Our combined paleoceanographic proxy data provide consistent descriptions of the ocean and sea ice conditions and ice-sheet/ocean interactions during deglaciation (Fig. 8). Furthermore, comparison of the proxy data with the GISP 2 $\delta^{18}O$ record indicates how the ice-sheet/ocean interactions that we document relate to the North Hemisphere climate history recorded in the Greenland summit ice core climate record (Fig. 8).

A parallel ocean-warming signal shown by the PC2 and PC3 in 12PC and VC46, respectively, provides strong evidence that subsurface ocean warming preceded (12PC) and accompanied ice retreat from the shelf edge. In both cores, the ocean-warming signal rose sharply by 17 cal ka BP and reached a peak at 16.2 cal ka BP (Fig. 8D, I). Increased productivity in 12PC prior to initial grounding line retreat is consistent with moderate opening in sea-ice cover (Supp. Fig. 3; Fig. 5B; 7B). The timing of the ocean-warming event coincides with, or slightly lags, Heinrich event 1 (c. 16.8 cal ka BP) from Hudson Strait (Hemming, 2004). Warm subsurface water during stadials and Heinrich events has been documented in the Nordic (Ezat et al., 2014) and Labrador seas (Marcott et al., 2011). Knutz et al. (2011) reported warm SSTs between 16.8 and 16.4 cal ka BP from southeastern Davis Strait reflecting IC advection (Fig. 8) that could also supply the warm subsurface water farther north along the CWG margin.

Ocean warming continued after 16.2 cal ka BP, with a second subsurface ocean-warming interval between 15.8 and 14.9 cal ka BP enveloping an IC advection event in SE Davis Strait (Knutz et al., 2011) (Fig. 8). This interval encompasses the transition from fine mud representing deposition in front of an ice shelf and pebbly mud reflecting the onset of calving retreat of the Disko and Uummannaq ice streams. In VC29, the peak warming between 15.4 and 15.2 cal ka BP (Fig. 8F) marks the end of strong ocean stratification and in-situ sea ice formation shown by the very light stable isotopic values in the planktic foraminifers (Fig. 6C) and the beginning of glacial meltwater fauna (Fig. 8F). The first calving retreat of the CWG grounding line followed Heinrich Event 1 and is somewhat later than initial grounding line retreat defined for the

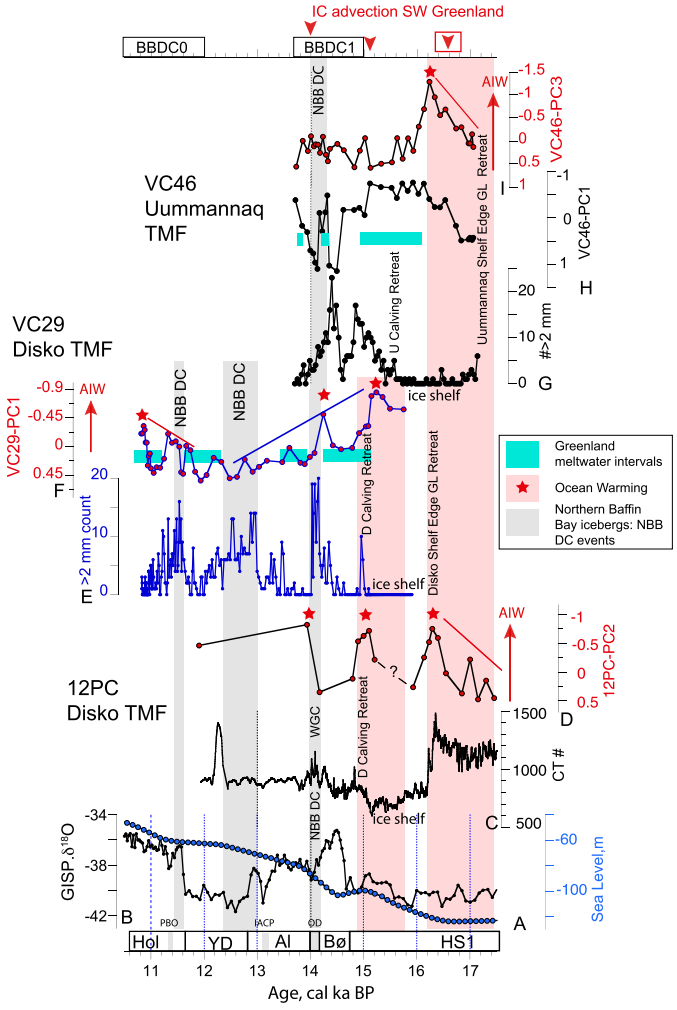

Fig. 8. Summary figure comparing key proxy records from VC46, VC29 and 12PC of iceberg rafting (C, E, G), ocean warming and cooling (D, F, I), meltwater (blue horizontal bars) and sediment provenance (gray bars) with GISP2 ice core δ^{18}O record (A) (Grootes et al., 1993), eustatic sea level (B) (Lambeck et al., 2014) and the interpreted timing of grounding line retreat, formation of the ice shelf, and calving retreat on the central West Greenland margin. Red stars indicate peaks of ocean warming. Red arrows indicate timing of IC advection events in core DA04-31P (Knutz et al., 2011). BBDC0 and BBDC1 timing from Simon et al., 2014. (For interpretation of the references to color in this figure legend, the reader is referred to the web version of this article.)

southern GIS margin (Knutz et al., 2011, 2013). If the 15.1 cal ka BP calving is correlative with the onset of the Bølling interstadial as has been suggested for the timing of IC advection by Knutz et al. (2011) for southern Greenland (Fig. 8F), it would require shifting the calibrated ages by 400 yrs, suggesting the need for a larger local reservoir correction (Fig. 8B).

A third warm peak is captured immediately before (VC29; Fig. 8F) and after (12PC; Fig. 8D) the first NBB DC event between 14.3 and 14.0 cal ka BP. This marks the end of the period of meltwater fauna associated with calving retreat of the Disko ice stream (Fig. 8F), the entry of chilled Atlantic Water species, *C. neoteretis*, into the benthic fauna (Supp. Fig. 3), and the beginning of consistent seasonal sea-ice occurrence (Fig. 5B). In VC46, a brief interval of warming and meltwater fauna occurs within the NBB DC event (Fig. 8A) and coincides with the MWP-1A (meltwater pulse 1A) from 14.5 to 14 cal ka BP (Lambeck et al., 2014). Together, these points signal the beginning of WGC and a seasonal sea-ice edge in Baffin Bay between 14.4 and 14.0 cal ka BP (Fig. 8). The first NBB DC event off CWG from 14.3 to 14.0 cal ka BP overlaps with BBDC 1 defined as 15.0–13.7 cal ka BP (Simon et al., 2014), and definitively lags Heinrich Event 1 (Andrews et al., 1998).

Ocean cooling and absence of a glacial meltwater fauna marks the NBB DC events from 14.2 cal ka BP onwards in VC29 (Fig. 8). In the three NBB DC intervals on West Greenland (14.3 to 14.0, 13.0 to 12.3, and 11.6 to 11.4 cal ka BP), IRD counts are high and meltwater fauna absent. Apart from 11.6–11.4 cal ka BP, these cold ocean periods coincide with cool periods in the GISP 2 ice core record (Fig. 8A), including the Older Dryas (GI-1d) and the Younger Dryas (GS-1) (Fig. 8). During the last two NBB DC events, *S. feylingi* is the dominant species, consistent with seasonal sea-ice formation (Seidenkrantz, 2013) off CWG, formed on NBB sourced freshwater (Supp. Fig. 5). The 3 intervals between the NBB DC events mark phases of CWG meltwater fauna and glacial marine sediment input (Fig. 8), suggesting that absence of the NBB meltwater input allows warming and melting of the GIS to prevail. In contrast, the presence of the cold freshwater from NBB appears to have dampened GIS melting and retreat.

7. Conclusions

We interpret multi-proxy sediment data to propose that CWG ice streams retreated from the shelf edge under the influence of subsurface, warm Atlantic Water that resided initially at depths below the ice sheet grounding lines (Fig. 7A). Ice retreat occurred either coincident with or shortly after Heinrich event 1. The deeper, Uummannaq ice stream, retreated first, while retreat of the Disko ice stream from the shelf edge was delayed until ca. 16.2 cal ka BP. Initial ice stream retreat did not produce IRD. We suggest that ice stream flow was buttressed by the presence of a fringing ice shelf, pervasive sea ice, and the level or normal (landward shallowing) bathymetry of the outer shelf. We do not explain the atmospheric or ocean circulation forcing that caused the subsurface warm ocean water to impinge on the grounding lines, but note that advection of warm IC water was observed at similar times upstream of the CWG cores, and that major changes in sea-surface conditions associated with Heinrich Event 1 may have played a role. Large-scale calving retreat was delayed until c. 15.1 cal ka BP, or slightly earlier in the Uummannaq system (15.3 cal ka BP), during a second interval of subsurface ocean warming.

Northern Baffin Bay ice sheet margins released several intervals of cold, fresh water and IRD during deglaciation. The freshwater release enhanced sea-ice formation and slowed melting and GIS retreat. This is especially apparent in the formation of a large grounding zone wedge in the Uummannaq Trough prior to, and during, the Younger Dryas (12.8–11.6 cal ka BP) (Sheldon et al., 2016; Dowdeswell et al., 2014). At this time, the CWG records document strong cooling, lack of GIS meltwater, and an increase in IRD from northern Baffin Bay.

The GIS remained grounded in the cross-shelf troughs until the early Holocene, when it retreated rapidly by calving and strong melting under the influence of atmosphere and ocean warming and a reverse bed slope into the adjoining bays and the deep fjords.

Acknowledgements

Funding for this research was provided by the US National Science Foundation grant ARC1203492 and the UK Natural Environment Research Council grant NE/D001951/1. We thank the officers crew and scientists aboard the RRS James Clark Ross during cruise JR175 to West Greenland in 2009 and the technical expertise of British Geological Survey personnel in core collection. We thank the captain, crew and scientists aboard the 2008 CSS Hudson cruise HU2008-029 for acquisition of core 2009029-12PC. We gratefully acknowledge the microscope and x-ray diffraction

research by undergraduate research assistants, Brian Shreve, Jennifer Kelly, Matthew Reed, Kelly Cox and Matthew Glasset. We gratefully acknowledge the helpful critique provided by 3 anonymous reviewers.

Appendix A. Supplementary material

Supplementary material related to this article can be found online at http://dx.doi.org/10.1016/j.epsl.2017.05.007.

References

Andrews, J.T., Eberl, D.D., 2011. Surface (sea floor) and near-surface (box cores) sediment mineralogy in Baffin Bay as a key to sediment provenance and ice sheet variations. Can. J. Earth Sci. 48 (9), 1307–1328. http://dx.doi.org/10.1139/-11-021.

Andrews, J.T., Eberl, D.D., 2012. Determination of sediment provenance by unmixing the mineralogy of source-area sediments: the "SedUnMix" program. Mar. Geol. 291, 24–33.

Andrews, J.T., Gibb, O.T., Jennings, A.E., Simon, Q., 2014. Variations in the provenance of sediment from ice sheets surrounding Baffin Bay during MIS 2 and 3 and export to the Labrador Shelf Sea: site HU2008029-0008 Davis Strait. J. Quat. Sci. 29, 3–13.

Andrews, J.T., Kirby, M.E., Aksu, A., Barber, D.C., Meese, D., 1998. Late quaternary detrital carbonate (DC-) layers in Baffin Bay Marine sediments (67°–74°N): correlation with Heinrich events in the North Atlantic? Quat. Sci. Rev. 17, 125–1137. http://dx.doi.org/10.1016/S0277-3791(97)00064-4.

Andrews, J.T., Osterman, L.E., Jennings, A.E., Syvitski, J.P.M., Miller, G.H., Weiner, N., 1996. Abrupt changes in marine conditions, Sunneshine Fiord, eastern Baffin Island, N.W.T. (ca. 66°N) during the last deglacial transition: Links to the Younger Dryas cold-event and Heinrich, H-0. In: Andrews, J.T., Austin, W., Bergsten, H., Jennings, H.E. (Eds.), Late Quaternary Paleoceanography of North Atlantic Margins. Geological Society of London, London, pp. 11–27.

Azetsu-Scott, K., Clarke, A., Falkner, K., Hamilton, J., Jones, P.E., Lee, C., Petrie, B., Prinsenberg, S., Starr, M., Yeats, P., 2010. J. Geophys. Res. 115, C11021. http://dx.doi.org/10.1029/2009JC005917.

Bamber, J.M., vanden Broeke, J., Ettema, J., Lenaerts, J., Rignot, E., 2012. Recent large increases in freshwater fluxes from Greenland into the North Atlantic. Geophys. Res. Lett. 39, L19501. http://dx.doi.org/10.1029/2012GL052552.

Belt, S.T., Massé, G., Rowland, S.J., Poulin, M., Michel, C., LeBlanc, B., 2007. A novel chemical fossil of palaeo sea ice: IP_{25}. Org. Geochem. 38, 16–27.

Buch, E., 2000a. A Monograph on the Physical Oceanography of the Greenland Waters. Danish Meteorological Institute Scientific Report, 00-12.

Buch, E., 2000b. Air–sea–ice conditions off southwest Greenland, 1981–1997. J. Northwest Atl. Fish. Sci. 26, 1–14.

Buch, E., Pedersen, S.A., Ribergaard, M.H., 2004. Ecosystem variability in West Greenland Waters. J. Northwest Atl. Fish. Sci. 34 (Part 2), 13–28.

Caralp, M.H., 1989. Size and morphology of the benthic foraminifer *Melonis barleeanum*: relationships with marine organic matter. J. Foraminiferal Res. 19, 235–245.

Corliss, B.H., 1991. Morphology and microhabitat preferences of benthic foraminifera from the northwest Atlantic Ocean. Mar. Micropaleontol. 17, 195–236.

Domack, E.W., Harris, P.T., 1998. A new depositional model for ice shelves, based upon sediment cores from the Ross Sea and the Mac. Roberson shelf, Antarctica. Ann. Glaciol. 27, 281–284.

Dowdeswell, J.A., Hogan, K.A., Ó Cofaigh, C., Fugelli, E.M.G., Evans, J., Noormets, R., 2014. Late Quaternary ice flow in a West Greenland fjord and cross-shelf trough system: submarine landforms from Rink Isbrae to Uummannaq shelf and slope. Quat. Sci. Rev. 92, 292–309. http://dx.doi.org/10.1016/j.quascirev.2013.09.007.

Enderlin, E.M., Howat, I.M., Jeong, S., Noh, M.-J., van Angelen, J.H., van den Broeke, M.R., 2014. An improved mass budget for the Greenland ice sheet. Geophys. Res. Lett. 41, 866–872. http://dx.doi.org/10.1002/2013GL059010.

England, J., Atkinson, N., Bednarski, J., Dyke, A.S., Hodgson, D.A., Ó Cofaigh, C., 2006. The Innuitian Ice Sheet: configuration, dynamics and chronology. Quat. Sci. Rev. 25, 689–703.

Evans, J., Dowdeswell, J.A., Grobe, H., Niessen, F., Stein, R., Hubberten, H.-W., Whittington, R.J., 2002. Late Quaternary sedimentation in Kejser Franz Joseph Fjord and the continental margin of East Greenland. In: Dowdeswell, J.A., Ó Cofaigh C (Eds.), Glacier-Influenced Sedimentation on High-Latitude Continental Margins. In: Geol. Soc. (Lond.) Spec. Publ., vol. 203, pp. 149–179.

Ezat, M.M., Rasmussen, T.L., Groeneveld, J., 2014. Persistent intermediate water warming during cold stadials in the southeastern Nordic Seas during the past 65 k.y. Geology 42, 663–666. http://dx.doi.org/10.1130/G35579.1.

Funder, S., Kjeldsen, K.K., Kjaer, K., Ó Cofaigh, C., 2011. The Greenland Ice Sheet during the past 300,000 years: a review. In: Ehlers, J., Gibbard, P.L., Hughes, P.D. (Eds.), Developments in Quaternary Sciences. Elsevier, Amsterdam, The Netherlands, pp. 699–713.

Grobe, H., 1987. A simple method for the determination of ice-rafted debris in sediment cores. Polarforschung 57 (3), 123–126.

Grootes, P.M., Stuiver, M., White, J.W.C., Johnsen, S., Jouzel, J., 1993. Comparison of oxygen isotope records from the GISP2 and GRIP Greenland ice cores. Nature 366, 552–554.

Hald, M., Korsun, S., 1997. Distribution of modern benthic foraminifera from fjords of Svalbard, European Arctic. J. Foraminiferal Res. 27, 101–122.

Hemming, S.R., 2004. Heinrich events: massive late Pleistocene detritus layers of the North Atlantic and their global climate imprint. Rev. Geophys. 42, RG1005.

Hillaire-Marcel, C., deVernal, A., 2008. Stable isotope clue to episodic sea ice formation in the glacial North Atlantic. Earth Planet. Sci. Lett. 268, 143–150.

Hofmann, J.C., Knutz, P.C., Nielsen, T., Kuijpers, A., 2016a. Seismic architecture and evolution of the Disko Bay trough-mouth fan, central West Greenland margin. Quat. Sci. Rev. http://dx.doi.org/10.1016/j.quascirev.2016.05.019.

Hofmann, J.C., Knutz, P., Ó Cofaigh C, 2016b. 3D-seismic observations of Late Pleistocene glacial dynamics on the central West Greenland margin. EGU2016-EGU15778.

Hogan, K.A., Dix, J.K., Lloyd, J.M., Long, A.J., Cotterill, C.J., 2011. Seismic stratigraphy records the deglacial history of Jakobshavn Isbræ, West Greenland. J. Quat. Sci. 26, 757–766.

Hogan, K.A., Ó Cofaigh, C., Jennings, A.E., Dowdeswell, J.A., Hiemstra, J.F., 2016. Deglaciation of a major palaeo-ice stream in Disko Trough, West Greenland. Quat. Sci. Rev. http://dx.doi.org/10.1016/j.quascirev.2016.01.018.

Höglund, H., 1947. Foraminifera in the Gullmar Fjord and the Skagerrak. Zool. Bidrag. Uppsala 26, 3–328.

Holland, D.M., Thomas, R.H., de Young, B., Ribergaard, M.H., Lyberth, B., 2008. Acceleration of Jakobshavn Isbræ triggered by warm subsurface oceanwaters. Nat. Geosci. 1 (10), 659–664. http://dx.doi.org/10.1038/ngeo316.

Jennings, A.E., Hald, M., Smith, L.M., Andrews, J.T., 2006. Freshwater forcing from the Greenland Ice Sheet during the Younger Dryas: evidence from southeastern Greenland shelf cores. Quat. Sci. Rev. 25, 282–298. http://dx.doi.org/10.1016/j.quascirev.2005.04.006.

Jennings, A.E., Helgadottir, G., 1994. Foraminiferal assemblages from the fjords and shelf of eastern Greenland. J. Foraminiferal Res. 24 (2), 123–144. http://dx.doi.org/10.2113/gsjfr.24.2.123.

Jennings, A.E., Sheldon, C., Cronin, T.M., Francus, F., Stoner, J., Andrews, J., 2011. The Holocene history of Nares Strait, transition from glacial bay to Arctic–Atlantic throughflow. Oceanography 24 (3), 26–41.

Jennings, A.E., Walton, M.E., Cofaigh, C.Ó., Kilfeather, A., Andrews, J.T., Ortiz, J.D., et al., 2014. Paleoenvironments during Younger Dryas–early Holocene retreat of the Greenland ice sheet from outer Disko Trough, central west Greenland. J. Quat. Sci. 29 (1), 27–40. http://dx.doi.org/10.1002/jqs.2652.

Jennings, A.E., Weiner, N.J., Helgadottir, G., Andrews, J.T., 2004. Modern foraminiferal faunas of the southwestern to northern Iceland shelf: oceanographic and environmental controls. J. Foraminiferal Res. 34, 180–207.

Joughin, I., Alley, R.B., Holland, D.M., 2012. Ice-sheet response to oceanic forcing. Science 338, 1172–1176.

Knudsen, K.L., Seidenkrantz, M.-S., 1994. *Stainforthia feylingi* new species from arctic to subarctic environments, previously recorded as *Stainforthia schreibersiana* (Czjzek). Spec. Pub. – Cushman Found. Foraminifer. Res. 32, 5–13.

Knutz, P.C., Sicre, M.-A., Ebbesen, H., Christiansen, S., Kuijpers, A., 2011. Multiple-stage deglacial retreat of the southern Greenland Ice Sheet linked with Irminger Current warm water transport. Paleoceanography 26, PA3204. http://dx.doi.org/10.1029/2010PA002053.

Knutz, P.C., Storey, M., Kuijpers, A., 2013. Greenland iceberg emissions constrained by $^{40}Ar/^{39}Ar$ horneblende ages: implications for ocean–climate variability during last deglaciation. Earth Planet. Sci. Lett. http://dx.doi.org/10.1016/j.epsl.2013.06.008.

Korsun, S., Polyak, L., 1989. Distribution of benthic foraminiferal morphogroups in the Barents Sea. Oceanology (Russia) 29, 838–844 (English translation).

Lambeck, K., Rouby, H., Purcell, A., Sun, Y., Sambridge, M., 2014. Sea level and global ice volumes from the Last Glacial Maximum to the Holocene. Proc. Natl. Acad. Sci. USA 111, 15296–15303.

Lane, T.P., Roberts, D.H., Rea, B.R., Ó Cofaigh, C., Vieli, A., Rodés, A., 2014. Controls upon the last glacial maximum deglaciation of the northern Uummannaq ice stream system, west Greenland. Quat. Sci. Rev. 92, 324–344. http://dx.doi.org/10.1016/j.quascirev.2013.09.013.

Larsen, N.K., Lecavalier, B., Bjørk, A.A., Colding, S., Huybrechts, P., Jakobsen, K.E., Kjeldsen, K.K., Knudsen, K.-L., Odgaard, B.V., Olsen, J., 2015. The response of the southern Greenland ice sheet to the Holocene thermal maximum. Geology 43 (4), 291–294. http://dx.doi.org/10.1130/G36476.1.

Lecavalier, B.S., Milne, G.A., Simpson, M.J.R., Wake, L., Huybrechts, P., Tarasov, L., Kjeldsen, K.K., Funder, S., Long, A.J., Woodroffe, S., Dyke, A.S., Larsen, N., 2014. A model of Greenland ice sheet deglaciation constrained by observations of relative sea level and ice extent. Quat. Sci. Rev. 102, 54–84.

Li, G., Piper, D.J.W., Campbell, D.C., 2011. The Quaternary Lancaster Sound trough-mouth fan, NW Baffin Bay. J. Quat. Sci. 26, 511–522.

Lloyd, J.M., 2006. Modern distribution of benthic foraminifera from Disko Bugt, West Greenland. J. Foraminiferal Res. 36, 315–331.

Lloyd, J.M., Moros, M., Perner, K., Telford, R.J., Kuijpers, A., Jansen, E., et al., 2011. A 100 yr record of ocean temperature control on the stability of Jakobshavn Isbrae, West Greenland. Geology 39 (9), 867–870. http://dx.doi.org/10.1130/G32076.1.

Marcott, S.A., et al., 2011. Ice-shelf collapse from subsurface warming as a trigger for Heinrich events. Proc. Natl. Acad. Sci. USA 108, 13415–13419. http://dx.doi.org/10.1107/pnas.1104772108.

Moon, T., Joughin, I., Smith, B., Howat, I., 2012. 21st-centry evolution of Greenland outlet glacier velocities. Science 336 (6081), 576–578. http://dx.doi.org/10.1126/science.1219985.

Nick, F.M., Vieli, A., Howat, I.M., Joughin, I., 2009. Large-scale changes in Greenland outlet glacier dynamics triggered at the terminus. Nat. Geosci. 394, 110–114.

Ó Cofaigh, C., Andrews, J.T., Jennings, A.E., Dowdeswell, J.A., Hogan, K.A., Kilfeather, A.A., Sheldon, C., 2013a. Glacimarine lithofacies, provenance and depositional processes on a West Greenland trough-mouth fan. J. Quat. Sci. 28. http://dx.doi.org/10.1002/jqs.2569.

Ó Cofaigh, C., Dowdeswell, J.A., Jennings, A.E., Hogan, K.A., Kilfeather, A., Hiemstra, J.F., et al., 2013b. An extensive and dynamic ice sheet on the West Greenland shelf during the last glacial cycle. Geology 41 (2), 219–222. http://dx.doi.org/10.1130/G33759.1.

Perner, K., Moros, M., Jennings, A., Lloyd, J.M., Knudsen, K.L., 2012. Holocene palaeoceanographic evolution off West Greenland. Holocene 23, 374–387.

Polyak, L., Korsun, S., Febo, L.A., Stanovoy, V., Khusid, T., Hald, M., Paulsen, B.E., Lubinski, D.J., 2002. Benthic foraminiferal assemblages from the southern Kara Sea, a river-influenced arctic marine environment. J. Foraminiferal Res. 32, 252–273.

Polyak, L., Solheim, A., 1994. Late- and postglacial environments in the northern Barents Sea west of Franz Josef Land. Polar Res. 13, 197–207.

Ramsey, C.B., Lee, S., 2013. Recent and planned developments of the program OxCal. Radiocarbon 55, 720–730.

Reimer, P.J., Bard, E., Bayliss, A., Beck, J.W., Blackwell, P.G., Ramsey, C.B., Grootes, P.M., Guilderson, T.P., Haflidason, H., Hajdas, I., Hatté, C., Heaton, T.J., Hoffmann, D.L., Hogg, A.G., Hughen, K.A., Kaiser, K.F., Kromer, B., Manning, S.W., Niu, M., Reimer, R.W., Richards, D.A., Scott, E.M., Southon, J.R., Staff, R.A., Turney, C.S.M., van der Plicht, J., 2013. IntCal13 and Marine13 radiocarbon age calibration curves 0–50,000 years cal BP. Radiocarbon 55, 1869–1887. http://dx.doi.org/10.2458/azu_js_rc.55.16947.

Ribergaard, M.H., Olsen, S.M., Mortensen, J., 2008. Oceanographic Investigations off West Greenland 2007. NAFO SCR Doc. 08/3, Scientific Council Meeting, June 2008.

Rignot, E., Fenty, I., Menemenlis, D., Xu, Y., 2012. Spreading of warm ocean waters around Greenland as a possible cause for glacier acceleration. Ann. Glaciol. 53 (60). http://dx.doi.org/10.3189/2012AoG60A136.

Rignot, E., Fenty, I., Xu, Y., Cai, C., Kemp, C., 2015. Under-cutting of marine-terminating glaciers in West Greenland. Geophys. Res. Lett. 42, 5909–5917. http://dx.doi.org/10.1002/2015GL064236.

Rignot, E., Mouginot, J., 2012. Ice flow in Greenland for the International Polar Year 2008–2009. Geophys. Res. Lett. 39, L11501. http://dx.doi.org/10.1029/2012GLO51634.

Roberts, D.H., Rea, B.R., Lane, T.P., Schnabel, C., Rodés, A., 2013. New constraints on Greenland ice sheet dynamics during the last glacial cycle: evidence from the Uummannaq ice stream system. J. Geophys. Res., Earth Surf. 118 (2), 519–541. http://dx.doi.org/10.1002/jgrf.20032.

Rytter, F., Knudsen, K.L., Seidenkrantz, M.-S., Eiríksson, J., 2002. Modern distribution of benthic foraminifera on the North Icelandic shelf and slope. J. Foraminiferal Res. 32, 217–244.

Schafer, C.T., Cole, F.E., 1986. Reconnaissance survey of benthonic foraminifera from Baffin Island fiord environments. Arctic 39, 232–239. http://dx.doi.org/10.14430/arctic2079.

Schafer, C.T., Cole, F.E., 1988. Environmental associations of Baffin Island fjord agglutinated foraminifera. Abh. Geol. Bundesanst. 307.

Schröder-Adams, C.J., Cole, F.E., Medioli, F.S., Mudie, P.J., Scott, D.B., Dobbin, L., 1990. Recent arctic shelf foraminifera: seasonally ice covered vs. perennially ice covered areas. J. Foraminiferal Res. 20, 8–36.

Scott, D.B., Vilks, G., 1991. Benthic foraminifera in the surface sediments of the deep sea Arctic ocean. J. Foraminiferal Res. 21, 20–38. http://dx.doi.org/10.2113/gsjfr.21.1.20.

Seidenkrantz, M.-S., 1995. *Cassidulina teretis* Tappan and *Cassidulina neoteretis* new species (Foraminifera): stratigraphic markers for deep sea and outer shelf areas. J. Micropaleontol. 14, 145–157. http://dx.doi.org/10.1144/jm.14.2.145.

Seidenkrantz, M.-S., 2013. Benthic foraminifera as palaeo sea-ice indicators in the subarctic realm-examples from the Labrador Sea-Baffin Bay region. Quat. Sci. Rev. 79, 135–144. http://dx.doi.org/10.1016/j.quascirev.2013.03.014.

Sheldon, C., Jennings, A., Andrews, J.T., Ó Cofaigh, C., Hogan, K., Dowdeswell, J.A., Seidenkrantz, M-S., 2016. Ice stream retreat following the LGM and onset of the west Greenland current in Uummannaq Trough, west Greenland. Quat. Sci. Rev. http://dx.doi.org/10.1016/j.quascirev.2016.01.019.

Simon, Q., Hillaire-Marcel, C., St-Onge, G., Andrews, J.T., 2014. Northeastern Laurentide, western Greenland and southern Innuitian ice stream dynamics during the last glacial cycle. J. Quat. Sci. 29 (1), 14–26. http://dx.doi.org/10.1002/jqs.2648.

Simon, Q., St-Onge, G., Hillaire-Marcel, C., 2012. Late Quaternary chronostratigraphic framework of deep Baffin Bay glaciomarine sediments from high-resolution paleomagnetic data. Geochem. Geophys. Geosyst. 13, Q0AO03. http://dx.doi.org/10.1029/2012GC004272.

Slubowska, M.A., Koç, N., Rasmussen, T.L., Klitgaard-Kristensen, D., 2005. Changes in the flow of Atlantic water into the Arctic Ocean since the last deglaciation: evidence from the northern Svalbard continental margin, 80 °C. Paleoceanography 20, PA4014. http://dx.doi.org/10.1029/2005PA001141.

Steinsund, P.I., 1994. Benthic Foraminifera in Surface Sediments of the Barents and Kara Seas: Modern and Late Quaternary Applications. Ph.D. dissertation. University of Tromsø. 111 pp.

Straneo, F., Heimbach, P., 2013. North Atlantic warming and the retreat of Greenland's outlet glaciers. Nature 504, 36–43. http://dx.doi.org/10.1038/nature12854.

Straneo, F., Sutherland, D.A., Holland, D., Gladish, C., Hamilton, G.S., Johnson, H.L., Rignot, E., Xu, Y., Koppes, M., 2012. Characteristics of ocean waters reaching Greenland's glaciers. Ann. Glaciol. 53 (60), 202–210. http://dx.doi.org/10.3189/2012AoG60A059.

Tang, C.C.L., Ross, C.K., Yao, T., Petrie, B., DeTracey, B.M., Dunlap, E., 2004. The circulation, water masses and sea-ice of Baffin Bay. Prog. Oceanogr. 63, 183–228.

Vasskog, K., Langebroek, P.M., Andrews, J.T., Ø Nilsen, J.E., Nesje, A., 2015. The Greenland Ice Sheet during the last glacial cycle: current ice loss and contribution to sea-level rise from a palaeoclimatic perspective. Earth-Sci. Rev. 150, 45–67.

Wollenburg, J.E., Mackensen, A., 1998. Living benthic foraminifera from the central Arctic Ocean: faunal composition, standing stock and diversity. Mar. Micropaleontol. 34, 153–185.

Wollenburg, J.E., Knies, J., Mackensen, A., 2004. High-resolution paleoproductivity fluctuations during the past 24 kyr as indicated by benthic foraminifera in the marginal Arctic Ocean. Palaeogeogr. Palaeoclimatol. Palaeoecol. 204, 209–238.

Zreda, M., England, J., Phillips, F., Elmore, D., Sharma, P., 1999. Unblocking of the Nares Strait by Greenland and Ellesmere Ice-Sheet retreat 10,000 years ago. Nature 398, 139–142. http://dx.doi.org/10.1038/18197.